

NUMERICAL SIMULATION OF CARDIAC MUSCLES IN A RAT BIVENTRICULAR MODEL

MINH TUẤN DƯƠNG^{1,3}, THERESA ACH¹, MUHANNAD ALKASSAR²,
SVEN DITTRICH² AND SIGRID LEYENDECKER¹

¹ Chair of Applied Dynamics, University of Erlangen Nuremberg
Immerwahrstrasse 1, 91058 Erlangen, Germany,
{minh.tuan.duong, sigrid.leyendecker}@fau.de and www.ltd.tf.uni-erlangen.de

² Pediatric Cardiology, University of Erlangen Nuremberg
LoschgestraÙe 15, 91054 Erlangen, Germany

³ School of Mechanical Engineering, Hanoi University of Science and Technology
1 DaiCoViet Road, Hanoi, Vietnam

Key words: Electromechanics, excitation-contraction, biventricular model, rat heart, myocardial infarction, FEM

Abstract. This paper presents the modelling and simulation of cardiac muscles in a rat biventricular model. Compared with the hugely advanced research on human hearts, the rat heart remains fairly little discussed so far. However, insights into rat heart function and heart failure may help to investigate human heart pathology. The biventricular model can produce a more realistic response of the rat heart compared with a separated left ventricle model. In this work, the excitation-induced contraction is modelled for the biventricular model with human heart parameters adapted for the faster heart rate of the rat. The passive mechanical properties of the model are formulated with an orthotropic exponential strain-energy function. Moreover, in partially and strongly coupled electromechanical problems, both excitation-induced contraction and mechano-electrical feedback interact with each other and this feedback is also able to alter the electrophysiology, which may mostly occur in diseased hearts, where deformations can be sufficiently high to induce excitation. Our computational model for the biventricular model is built up based on a three-dimensional (3D) geometry from magnetic resonance imaging (MRI) and then developed with an approximated fibre orientation map. The electromechanically coupled problem of cardiac muscle contractions of the rat heart is subsequently solved using a fully implicit finite element-based monodomain framework associated with the stress approach. Our numerical results for a healthy and an infarcted case show the capability of our electromechanical model to be an essential protocol to investigate rat heart pathology.

1 INTRODUCTION

Despite largely significant developments in heart pathology, cardiovascular diseases remain the major causes of human death in the world. In addition, it has been ever nontrivial to fully access the cardiac electromechanics due to the complexity of cardiac structure and its mechanics and electrophysiology as well as the challenge in performing experiments *'in-vivo'*. Inspired by these difficulties, computational models are therefore developed as effective tools for not only gaining deeper insights into the heart function and heart failure but also testing/designing therapy and especially constructing cardiac devices [1, 2].

Many studies have first focused on the human left ventricle since it creates the main pumping force and its functional failure takes place more often and then significantly affects the heart function. However, including the right ventricle in modelling importantly helps to investigate its roles and certainly results in a more accurate response of the model [3]. Thus, biventricular models have been paid special attention such as in the following studies. Since the cardiac mechanics is complicated due to heterogeneity of cardiac muscles and their orientation distribution as well as contraction behaviour, the passive mechanics is therefore modelled as anisotropic behaviour such as characterized by the Fung-type model [4], a transversely isotropic model [5] or by the orthotropic material laws with and without fibre dispersion [6, 7]. Additionally, based on the fibre-sheet structure of the myocardium in which the fibres are helically distributed around the longitudinal axis of the biventricular model, the active stress or excitation contraction formulation can be modelled along the fibre direction (one-dimensional) [5], the fibre and sheet directions (two-dimensional) [1] and the fibre, sheet and normal directions (three-dimensional) [8]. The cardiac electrophysiology is widely characterized by the ionic Hodgkin-Huxley model for neurons [9]. Based on the Hodgkin-Huxley description, the Aliev-Panfilov and the FitzHugh-Nagumo models are derived and preferably used to simulate nonpacemaker cells and pacemaker cells in living hearts, respectively [10, 11]. These models are also useful to study, in particular, atrial and ventricular fibrillation. Unlike the excitation-induced contraction, myocytes can also be excited through the stretch-induced opening of ion channels [12]. Coupled, decoupled and staggered methods can be used to solve the electromechanical problems [1, 5, 13]. In contrast to huge developments in modelling human hearts, research on rat hearts is relatively narrowed to a certain extent. The electrophysiology of a rat is modelled by an ionic model associated with transmural heterogeneity [14] and the impact of fibre orientations on the ventricular electromechanics is presented in [4]. Furthermore, the fibre orientation for rat hearts can be constructed using high-resolution diffusion tensor imaging [15]. Passive mechanical properties of infarcted rat myocardium at different time points have been characterized by mechanical tension and compression tests in [16]. Obviously, there is still lacking in numerical experiments on infarcted hearts.

In this paper, we present a general procedure to formulate and solve partially/strongly coupled electromechanical problems of cardiac muscles for a rat, which is still undiscussed in detail for rats and lacks of computational implementation and numerical studies [2, 17]. Fortunately, the cardiac mechanisms of a rat and human are similar, hence, many mathe-

mathematical descriptions of the cardiac physiology can be transferred by scaling and adjusting relevant parameters [18]. Our study explores the effective electromechanical model based on a biventricular 3D geometry of a rat heart obtained from the Universitätsklinikum Erlangen-Nuremberg. We also investigate the capability of this model to study the rat heart pathology (infarcted heart) and its possibility to support designs of cardiac devices.

2 GOVERNING EQUATIONS

2.1 Kinematics

Let us consider a deformable and excitable body $\Omega_0 \subset \mathbb{R}^3$ that deforms to the current configuration $\Omega \subset \mathbb{R}^3$ at $t > t_0$. Material points $\mathbf{X} \in \Omega_0$ move to their spatial positions $\mathbf{x} \in \Omega$ through the non-linear deformation map $\mathbf{x} = \boldsymbol{\varphi}(\mathbf{X}, t)$. Thus the deformation gradient is defined as $\mathbf{F} = \frac{\partial \boldsymbol{\varphi}(\mathbf{X}, t)}{\partial \mathbf{X}} = \nabla \boldsymbol{\varphi}(\mathbf{X}, t)$ and $J = \det \mathbf{F} > 0$ and $\mathbf{C} = \mathbf{F}^T \mathbf{F}$ is the right Cauchy-Green tensor.

2.2 Balance equations and boundary value problem

For electromechanically coupled problems with two primary field variables, placement $\boldsymbol{\varphi}(\mathbf{X}, t)$ and action potential (AP) $\Phi(\mathbf{X}, t)$, there exist two field equations which govern the state of the material points \mathbf{X} at time t . The mechanical field equation is derived by the balance of linear momentum as

$$\mathbf{0} = \text{Div}[\mathbf{F} \cdot \mathbf{S}] + \mathbf{F}^\varphi \quad \text{in } \Omega_0, \quad (1)$$

where \mathbf{S} is the second Piola-Kirchhoff stress tensor and \mathbf{F}^φ is the external mechanical body force. The evolution of the transmembrane AP Φ can be written as

$$\dot{\Phi} = \text{Div}[\mathbf{Q}] + F^\Phi \quad \text{in } \Omega_0. \quad (2)$$

where the non-linear current term is F^Φ , whereas $\dot{\Phi}$ denotes the material time derivative of the action potential field Φ , and \mathbf{Q} is the electrical potential flux vector. The Neumann and Dirichlet conditions are $\mathbf{Q} \cdot \mathbf{N} = \bar{Q}$ on Γ_Q , $\mathbf{T} = \bar{\mathbf{T}}$ on Γ_T , and $\varphi = \bar{\varphi}$ on Γ_φ , respectively. Similarly, we have initial conditions $\Phi(\mathbf{X}, 0) = \bar{\Phi}$ on Γ_Φ , see Figure 1.

3 CONSTITUTIVE EQUATIONS

3.1 Mechanical model

In this section, the stress approach is described as it is divided into a passive and an active part.

$$\mathbf{S} = \mathbf{S}^{pas}(\boldsymbol{\varphi}) + \mathbf{S}^{act}(\boldsymbol{\varphi}, \Phi) \quad (3)$$

From the strain-energy function Ψ the associated mechanical constitutive equations can be derived as follows

$\mathbf{S} = 2 \frac{\partial \Psi}{\partial \mathbf{C}}$, and the Cauchy stress $\boldsymbol{\sigma} = \mathcal{X}_*(\mathbf{S}) = \frac{1}{J} \mathbf{F} \cdot \mathbf{S} \cdot \mathbf{F}^T$, where $\mathcal{X}_*(\circ)$ denotes the push-forward of (\circ) from its material configuration to the spatial one.

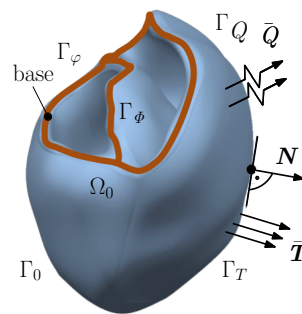


Figure 1: Boundary surface $\Gamma_0 = \Gamma_\varphi \cup \Gamma_T$ and $\Gamma_0 = \Gamma_\Phi \cup \Gamma_Q$.

Passive stress response The Holzapfel-Ogden (H-O) model is employed for describing the passive mechanical response of the incompressible hyperelastic orthotropic myocardium tissue [6]. This model can characterize the fibre-sheet structure with the fibre direction \mathbf{f}_0 and the sheet direction \mathbf{s}_0 and has the form

$$\begin{aligned} \Psi = & \frac{a}{2b} \exp[b(\bar{I}_1 - 3)] + \sum_{i=f,s} \frac{a_i}{2b_i} \left\{ \exp[b_i(\bar{I}_{4i} - 1)^2] - 1 \right\} \\ & + \frac{a_{fs}}{2b_{fs}} \left[\exp(b_{fs} \bar{I}_{8fs}^2) - 1 \right], \end{aligned} \quad (4)$$

where $i \in \{f, s\}$ and the variables $a, b, a_f, b_f, a_s, b_s, a_{fs}, b_{fs}$ are material constants. While all a, a_f, a_s, a_{fs} parameters have the dimension of stress, all b, b_f, b_s, b_{fs} are dimensionless. These quantities are derived from the isochoric deformation gradient $\bar{\mathbf{C}} = \bar{\mathbf{F}}^T \bar{\mathbf{F}}$, where the deformation gradient can be split into two parts as $\mathbf{F} = (J^{1/3} \mathbf{I}) \bar{\mathbf{F}}$ where \mathbf{I} is the identity tensor. Specifically, $J^{1/3} \mathbf{I}$ describes purely volumetric deformation whereas $\bar{\mathbf{F}}$ denotes the purely isochoric deformation ($\bar{J} = \det(\bar{\mathbf{F}}) = 1$). The principal isochoric invariants of $\bar{\mathbf{C}}$ are defined as $\bar{I}_1(\bar{\mathbf{C}}) = \text{tr}(\bar{\mathbf{C}})$, $\bar{I}_{4f}(\bar{\mathbf{C}}) = \mathbf{f}_0 \cdot (\bar{\mathbf{C}} \mathbf{f}_0)$, $\bar{I}_{4s}(\bar{\mathbf{C}}) = \mathbf{s}_0 \cdot (\bar{\mathbf{C}} \mathbf{s}_0)$, and $\bar{I}_{8fs}(\bar{\mathbf{C}}) = \mathbf{f}_0 \cdot (\bar{\mathbf{C}} \mathbf{s}_0)$. In addition, the standard and isochoric fibre and sheet direction vectors in the material are $\mathbf{f}_0, \bar{\mathbf{f}}_0 = (J^{-1/3}) \mathbf{f}_0, \mathbf{s}_0$ and $\bar{\mathbf{s}}_0 = (J^{-1/3}) \mathbf{s}_0$, and in the current configuration, $\mathbf{f}, \bar{\mathbf{f}}, \mathbf{s}$ and $\bar{\mathbf{s}}$. The passive second Piola-Kirchhoff stress is evaluated as $\mathbf{S}^{pas} = \mathbf{S}_{iso} + \mathbf{S}_{ani}$, where

$$\begin{aligned} \mathbf{S}_{iso} &= a \exp[b(\bar{I}_1 - 3)] \left(J^{-2/3} \mathbf{I} - \frac{1}{3} \bar{I}_1 \mathbf{C}^{-1} \right) \\ \mathbf{S}_{ani} &= \sum_{i=f,s} 2(\bar{I}_{4i} - 1) a_i \exp[b_i(\bar{I}_{4i} - 1)^2] \left(\bar{\mathbf{i}}_0 \otimes \bar{\mathbf{i}}_0 - \frac{1}{3} \bar{I}_{4i} \mathbf{C}^{-1} \right) \\ &+ \bar{I}_{8fs} a_{fs} \exp(b_{fs} \bar{I}_{8fs}^2) \left[(\bar{\mathbf{f}}_0 \otimes \bar{\mathbf{s}}_0 + \bar{\mathbf{s}}_0 \otimes \bar{\mathbf{f}}_0) - \frac{2}{3} \bar{I}_{8fs} \mathbf{C}^{-1} \right]. \end{aligned} \quad (5)$$

Active stress response The cardiac muscle contraction induced by an electrical excitation is described by the active part of the second Piola-Kirchhoff stress tensor \mathbf{S}^{act} or the Cauchy stress tensor $\boldsymbol{\sigma}^{act}$. Reaching a certain threshold in the AP, the cell starts to shrink and initiate the final pumping mechanism of the rat heart. Taking into account the fibre orientation \mathbf{f}_0 and the sheet plane direction \mathbf{s}_0 yields

$$\mathbf{S}^{act}(\mathbf{C}, \mathbf{f}_0, \mathbf{s}_0, \Phi) = T^{act}(\Phi) \left[I_{4f}^{-1} \nu_{ff} \mathbf{f}_0 \otimes \mathbf{f}_0 + I_{4s}^{-1} \nu_{ss} \mathbf{s}_0 \otimes \mathbf{s}_0 \right], \quad (6)$$

where $I_{4f} = \mathbf{C} : (\mathbf{f}_0 \otimes \mathbf{f}_0) = \lambda^2$, $I_{4s} = \mathbf{C} : (\mathbf{s}_0 \otimes \mathbf{s}_0)$, ν_{ff} and ν_{ss} are weighting factors and the active fibre tension T^{act} is computed from its evolution equation as $\dot{T}^{act} = T(\Phi, T^{act})$ specified in section 6.1.

3.2 Electrophysiological constitutive models

The current source term F^Φ is split into two parts as $F^\Phi = F_e^\Phi(\Phi, r) + F_m^\Phi(\boldsymbol{\varphi}, \Phi)$, where F_e^Φ expresses the purely electrical part and F_m^Φ accounts for possible mechanically-induced excitation (MEF), and r denotes the recovery variable of the cellular excitation which is later solved internally. The excitation-induced purely electrical part F_e^Φ describes the effective current generation due to the inward and outward flow of ions across the cell

membrane. This ionic flow is triggered by a perturbation of the resting potential of a cardiac cell beyond some physical threshold upon the arrival of the depolarization front [5, 11]. The purely electrical model is written as

$$F_e^\Phi = c\Phi(\Phi - \alpha)(1 - \Phi) - r\Phi + I, \quad (7)$$

where the variables α and c are material parameters, α controls the oscillation threshold, c is a scaling parameter, I is an external stimulus and $\dot{r} = f^r(\Phi, r)$, see section 6.2.

Mechano-electrical feedback (MEF) The stretch-induced mechano-electrical part F_m^Φ incorporates the opening of ion channels under the action of deformation. This behaviour is observed due to stretch-induced opening of ion channels which induces electrical potential generation. It is described by the constitutive equation for the electrical source term as $F_m^\Phi = \vartheta G_s (\lambda - 1) (\Phi_s - \Phi)$, where G_s denotes the maximum conductance, Φ_s the resting potential, $\vartheta = 1$ when $\lambda = \sqrt{I_{4f}} > 0$ and $\vartheta = 0$ otherwise [19].

Potential flux In the case of linear diffusion the electrical flux is proportional to the current gradient of the electrical field $\nabla_x \Phi$. When referred to the material configuration, the electrical flux has the form $\mathbf{Q} = \mathbf{D} \cdot \nabla \Phi$ with the conductivity tensor $\mathbf{D} = D_{iso} \mathbf{C}^{-1} + D_{ani} \mathbf{f}_0 \otimes \mathbf{f}_0$, where D_{iso} and D_{ani} are constants.

4 INFARCTED RAT MYOCARDIUM

Myocardial infarction (MI) is considered as a major cause of death. Thrombosis and coronary artery atherosclerosis are the main causes of MI and precipitate local ischemia and necrosis of myocardial cells [20]. In this work, we discuss the lateral MI (transmural infarct) which mostly occurs in the myocardium due to occlusion of the left circumflex artery. The size and the position of the infarcted region for our numerical simulations are illustrated in Figure 2. There is few living cells and the conductivity of the infarcted region is relatively close to the zero value which slows down the electrical wave transmission.

Consequently, since most of the cells are dead, the infarcted region does not contract and is found to be stiffer than the healthy region of rat hearts [16]. Furthermore, the volume during the diastolic phase in an infarcted canine left ventricle is found to be smaller than the healthy one [21]. Thus, when the cardiac muscles in the infarcted heart loose their function, less blood is pumped to the body. Herein, we consider the transmural infarct case in which the thickness of the infarcted region is assumed to be unchanged.

5 FINITE ELEMENT FORMULATION

In this section, a standard finite element procedure is used to approximately solve the initial and boundary value problem. In the following, to solve the governing equations, we



Figure 2: Lateral MI region.

first rewrite the nonlinear problem in its weak form and then discretize it with a finite difference scheme in time and a finite element scheme in space.

5.1 Weak form of electromechanical problem

Following the Galerkin procedure, the residuals R^Φ and \mathbf{R}^φ are multiplied with the scalar- and vector-valued test functions $\delta\Phi$ and $\delta\varphi$ which satisfy $\delta\varphi = \mathbf{0}$ on Γ_φ and $\delta\Phi = 0$ on Γ_Φ , respectively and integrated over the reference domain to yield

$$\begin{aligned} G^\Phi &= \int_{\Omega_0} \delta\Phi \dot{\Phi} dV + \int_{\Omega_0} \nabla(\delta\Phi) \cdot \mathbf{Q} dV - \int_{\Omega_0} \delta\Phi F^\Phi dV - \int_{\Gamma_Q} \delta\Phi \bar{Q} da \doteq 0 \\ G^\varphi &= \int_{\Omega_0} \nabla(\delta\varphi) : [\mathbf{F} \cdot \mathbf{S}] dV - \int_{\Omega_0} \delta\varphi \cdot \mathbf{F}^\varphi dV - \int_{\Gamma_T} \delta\varphi \cdot \bar{\mathbf{T}} da \doteq 0. \end{aligned} \quad (8)$$

Herein, the Dirichlet boundary conditions prescribe the state of the respective surface points to be equal to $\bar{\varphi}$ and $\bar{\Phi}$ and the Neumann boundary conditions prescribe the surface traction $\bar{\mathbf{T}}$ and the surface flux term \bar{Q} . These quantities as well as the external forces \mathbf{F}^φ and current F^Φ are all supposed to be given.

5.2 Temporal and spatial discretization

We need to have the temporal discretization, the observation time $\mathcal{T} = [0, t]$ of the electromechanical problem is partitioned into n_{step} periods $[t_n, t_{n+1}]$ of length $\Delta t = t_{n+1} - t_n$, i.e. $\mathcal{T} = \bigcup_{n=1}^{n_{step}} [t_n, t_{n+1}]$ and an implicit Euler scheme with $\dot{\Phi} \approx \frac{\Phi_{n+1} - \Phi_n}{\Delta t}$. For the sake of simplicity, the index 'n + 1' is suppressed in all equations. The spatial discretization is implemented by dividing the body Ω_0 into n_{el} finite elements $\Omega_{0,e}^h$ so that $\Omega_0 \approx \Omega_0^h = \bigcup_{e=1}^{n_{el}} \Omega_{0,e}^h$. The field variables φ and Φ and their test functions $\delta\varphi$ and $\delta\Phi$ can then be approximated on each element $\Omega_{0,e}^h$ with the number of nodes per element n_{ne} and shape functions $N^i(\mathbf{X})$ for $i = 1 \dots n_{ne}$ as $\delta\Phi_e^h = \sum_{i=1}^{n_{ne}} N^i \delta\Phi_i^e$, $\delta\varphi_e^h = \sum_{j=1}^{n_{ne}} N^j \delta\varphi_j^e$, $\Phi_e^h = \sum_{k=1}^{n_{ne}} N^k \Phi_k^e$, and $\varphi_e^h = \sum_{l=1}^{n_{ne}} N^l \varphi_l^e$. Similarly, explicit forms for the increments for a consistent linearization and the Newton-Raphson scheme are expressed as $\Delta\Phi_e^h = \sum_{i=1}^{n_{ne}} N^i \Delta\Phi_i^e$, $\Delta\varphi_e^h = \sum_{j=1}^{n_{ne}} N^j \Delta\varphi_j^e$, $\nabla(\Delta\Phi_e^h) = \sum_{k=1}^{n_{ne}} \nabla N^k \Delta\Phi_k^e$, and $\nabla(\Delta\varphi_e^h) = \sum_{l=1}^{n_{ne}} \Delta\varphi_l^e \otimes \nabla N^l$. The nonlinear boundary value problem in the residual weak form (8) associated with the boundary flux term $\bar{Q} = 0$ can then be reformulated with the temporal and spatial discretization as

$$\begin{aligned} R_I^\Phi &= \mathbf{A}_{e=1}^{n_{el}} \left\{ \int_{\Omega_{0,e}^h} N^i \frac{\Phi - \Phi_n}{\Delta t} dV + \int_{\Omega_{0,e}^h} \nabla N^i \cdot \mathbf{Q} dV - \int_{\Omega_{0,e}^h} N^i F^\Phi dV \right\} \doteq 0 \\ \mathbf{R}_J^\varphi &= \mathbf{A}_{e=1}^{n_{el}} \left\{ \int_{\Omega_{0,e}^h} \nabla N^j \cdot \mathbf{F} \cdot \mathbf{S} dV - \int_{\Omega_{0,e}^h} N^j \mathbf{F}^\varphi dV - \int_{\Gamma_T^e} N^j \bar{\mathbf{T}} dA \right\} \doteq \mathbf{0}, \end{aligned} \quad (9)$$

where \mathbf{A} represents the assembly operator. All element residuals at the local element nodes i and j are added to the global residuals at the global nodes I and J . Herein, $i, j = 1, \dots, n_{en}$ and $I, J = 1, \dots, n_{nd}$, where n_{nd} is the number of nodes in the body mesh.

5.3 Linearisation and iterative solver

In order to solve the discrete non-linear boundary value problem for its nodal field variables (AP Φ_I and deformation φ_J), a consistent linearisation is required. Specifically, the residuals are linearized along the increments $\Delta\Phi$ and $\Delta\varphi$ to yield

$$\begin{aligned} \mathbf{R}_I^\Phi + \sum_K \mathbf{K}_{IK}^{\Phi\Phi} \Delta\Phi_K + \sum_L \mathbf{K}_{IL}^{\Phi\varphi} \cdot \Delta\varphi_L &\doteq \mathbf{0} \\ \mathbf{R}_J^\varphi + \sum_K \mathbf{K}_{JK}^{\varphi\Phi} \Delta\Phi_K + \sum_L \mathbf{K}_{JL}^{\varphi\varphi} \cdot \Delta\varphi_L &\doteq \mathbf{0} \end{aligned} \quad (10)$$

In (10) the iteration matrices $\mathbf{K}_{IK}^{\Phi\Phi}$, $\mathbf{K}_{IL}^{\Phi\varphi}$, $\mathbf{K}_{JK}^{\varphi\Phi}$ and $\mathbf{K}_{JL}^{\varphi\varphi}$ are obtained as

$$\begin{aligned} \mathbf{K}_{IK}^{\Phi\Phi} &= \mathbf{A}_{e=1}^{nel} \int_{\Omega_{0,e}^h} \nabla N^i \cdot \mathbf{D} \cdot \nabla N^k dV + \int_{\Omega_{0,e}^h} N^i \left(\frac{1}{\Delta t} - d_\Phi F^\Phi \right) N^k dV \\ \mathbf{K}_{IL}^{\Phi\varphi} &= \mathbf{A}_{e=1}^{nel} \int_{\Omega_{0,e}^h} 2 \left(N^i d_{\mathbf{C}} F^\Phi + \nabla N^i d_{\mathbf{C}} \mathbf{Q} \right) (\mathbf{F}^T \cdot \nabla N^l)^{sym} dV \\ \mathbf{K}_{JK}^{\varphi\Phi} &= \mathbf{A}_{e=1}^{nel} \int_{\Omega_{0,e}^h} \nabla N^j \cdot \mathbf{F} d_\Phi \mathbf{S}^{act} N^k dV \\ \mathbf{K}_{JL}^{\varphi\varphi} &= \mathbf{A}_{e=1}^{nel} \int_{\Omega_{0,e}^h} (\nabla N^j \cdot \mathbf{F})^{sym} : 2d_{\mathbf{C}} \mathbf{S} : (\mathbf{F}^T \cdot \nabla N^l)^{sym} dV. \end{aligned} \quad (11)$$

The operators are $[\circ]^{sym} = \frac{1}{2}([\circ] + [\circ]^T)$ and the total derivative $d_{[\circ]}(\circ) = d(\circ)/d[\circ]$. By using the Newton-Raphson methods, an iterative solution scheme updates the global unknowns $\Phi_I \leftarrow \Phi_I + \Delta\Phi_I$ and $\varphi_J \leftarrow \varphi_J + \Delta\varphi_J$.

6 INTERNAL VARIABLES AND SENSITIVITIES

To complete the iteration matrices, evolution of internal variables and the sensitivities or partial derivatives must be computed.

6.1 Active stress response

The evolution for the muscle traction is $\dot{T}^{act} = \epsilon(\Phi) [k_T (\Phi - \Phi_r) - T^{act}]$ with its sensitivity to the AP $\frac{\partial \mathbf{S}^{act}}{\partial \Phi} = \partial_\Phi T^{act}(\Phi) [I_{4f}^{-1} \nu_{ff} \mathbf{f}_0 \otimes \mathbf{f}_0 + I_{4s}^{-1} \nu_{ss} \mathbf{s}_0 \otimes \mathbf{s}_0]$, where k_T specifies the saturated value of $T^{act}(\Phi)$, Φ_r is the resting potential where no new tension is evoked (for cardiac cells usually around -80mV), and $\epsilon(\Phi)$ represents the switch function as $\epsilon(\Phi) = \epsilon_0 + (\epsilon_\infty - \epsilon_0) \exp \left[- \exp \left(-\xi \left(\Phi - \tilde{\Phi} \right) \right) \right]$. The special behaviour can be adjusted by the parameters ϵ_0 and ϵ_∞ which regulate the limitation values $\tilde{\Phi}$ denoting the phase shift and ξ controlling the transition rate from ϵ_0 to ϵ_∞ , see [22]. The impact of the active fibre tension on the active stress along the fibre direction and in sheet direction are controlled by ν_{ff} and ν_{ss} , respectively. T^{act} can be treated as an internal variable and has to be solved internally. The temporal discretization of the time derivative reads $\dot{T}^{act} \approx \frac{T^{act} - T_n^{act}}{\Delta t}$. Here, T^{act} denotes the active fibre tension at time t_{n+1} , while T_n^{act} is the active fibre tension at t_n . By these specifications, the residual $R^T = T^{act} - T_n^{act} - \Delta t \epsilon(\Phi) [k_T (\Phi - \Phi_r) - T^{act}] \doteq 0$ has to vanish. The sensitivities of the potential flux and the second Piola-Kirchhoff stress tensor with respect to the deformation can be found as $d_{\mathbf{C}} \mathbf{Q} = \{D_{iso} \frac{1}{2} [\mathbf{C}^{-1} \bar{\otimes} \mathbf{C}^{-1}] + D_{ani} I_{4f}^{-2} (\mathbf{f}_0 \otimes \mathbf{f}_0) \otimes (\mathbf{f}_0 \otimes \mathbf{f}_0)\} \cdot \nabla \Phi$.

The constitutive tensor can be computed in a straightforward way as $d_{\mathbf{C}}\mathbf{S} = \frac{\partial \mathbf{S}}{\partial \mathbf{C}} = 2 \frac{\partial^2 \Psi}{\partial \mathbf{C}^2}$. For conciseness, we do not explicitly write its form here.

6.2 Electrophysiological model

The recovery variable r is governed by the local ordinary differential equation as

$$\dot{r} = f^r = \left[\gamma + \frac{\mu_1 r}{\mu_2 + \Phi} \right] [-r - c\Phi(\Phi - \beta - 1)] \quad (12)$$

The time derivative \dot{r} denotes the change in the recovery variable r and the variables μ_1 , μ_2 , β and γ are additional material parameters. While the coefficient term $\left[\gamma + \frac{\mu_1 r}{\mu_2 + \Phi} \right]$ is a weighting factor, β controls the AP duration. Considering the boundary value problem (8), r can be treated as an internal variable. In order to solve the internal evolution equation (12), the implicit Euler method is used. Hence, the residual can be introduced as $R^r = r - r_n - \Delta t f^r(\Phi, r) \doteq 0$ with the sensitivity $\partial_r R^r = 1 + \Delta t \left[\gamma + \frac{\mu_1}{\mu_2 + \Phi} [2r + c\Phi(\Phi - \beta - 1)] \right]$. The term $d_{\Phi} F^{\Phi}$ is written as $d_{\Phi} F^{\Phi}(\mathbf{C}, \Phi, r) = d_{\Phi} F_e^{\Phi} + d_{\Phi} F_m^{\Phi} = \frac{\partial F_e^{\Phi}}{\partial \Phi} + \frac{\partial F_e^{\Phi}}{\partial r} \frac{dr}{d\Phi} + \frac{dF_m^{\Phi}}{d\Phi}$.

As $R^r = 0$ is consistently fulfilled throughout the whole equation system, $d_{\Phi} R^r = \partial_{\Phi} R^r + \partial_r R^r d_{\Phi} r \doteq 0$ has to hold. Thus, $d_{\Phi} r$ can be obtained as $d_{\Phi} r = -(\partial_r R^r)^{-1} \partial_{\Phi} R^r$ with $\partial_{\Phi} R^r$ evaluated as $\partial_{\Phi} R^r = \Delta t \left[\left[\gamma + \frac{\mu_1 r}{\mu_2 + \Phi} \right] c(2\Phi - \beta - 1) - \frac{\mu_1 r}{(\mu_2 + \Phi)^2} [r + c\Phi(\Phi - \beta - 1)] \right]$.

In Figure 3, the AP evolution of a cardiac cell continuum is displayed alongside the recovery variable against time. Here, the normalized governing equation for the AP is iteratively solved using an implicit Euler scheme with Newton-Raphson method. To trigger the AP excitation, a stimulus I is required as the model is not self-oscillating. In Figure 3, the AP then increases suddenly and steep in the depolarization phase. After reaching its maximum value of 1.0 and the plateau period (around the absolute refractory period), the repolarization follows and it smoothly returns to its resting potential. We adapt this model for rat hearts with new parameters given in the caption of Figure 3. The

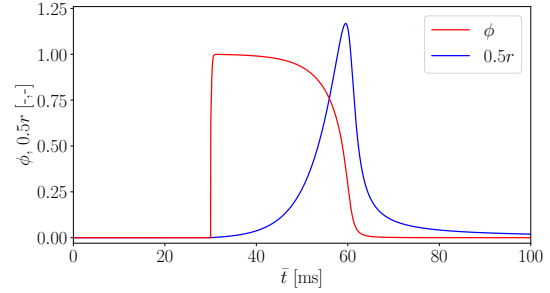


Figure 3: Evolution of normalized AP ϕ and recovery variable $0.5r$ over normalized time \bar{t} with $\alpha = 0.01$, $\gamma = 0.002$, $\beta = 0.55$, $c = 8$, $\mu_1 = 0.2$ and $\mu_2 = 0.3$, and a stimulus $I = 30$ at $\bar{t} = 30$ to trigger cardiac cell.

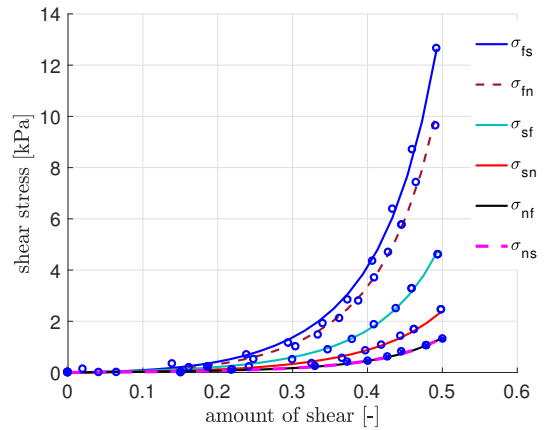


Figure 4: Fitted parameters for simple shear data modified for rat heart.

tangent terms of the mechano-electrical feedback F_m^Φ with respect to AP and deformation, respectively read $\partial_\Phi F_m^\Phi = -\vartheta G_s (\lambda - 1)$ and $d_C F^\Phi = \frac{1}{2} \vartheta G_s (\Phi_s - \Phi) \lambda^{-1} \mathbf{f}_0 \otimes \mathbf{f}_0$.

7 NUMERICAL RESULTS

Material parameters In this section, numerical simulations of the biventricular model of a rat are presented to demonstrate the capability of the current computational model. Therefore, parameters for the whole model need to be estimated and adapted by our parameter study such that the characteristics of electromechanics of the faster than human heart rate can be represented. Firstly, the material parameters for the passive mechanics of the rat are obtained by curve fitting to experimental porcine data in [23], which were scaled down with a factor of 0.8, see Figure 4. This factor is roughly computed by comparing the scaled data with experimental data for rats in biaxial mechanical tests in [16]. Similarly, material coefficients for the infarcted region can be obtained by the same fitting procedure with an assumed factor of 2.5 due to the fact that this region is stiffer since it lacks of fresh blood and oxygen. Secondly, the parameters for the electrical model and active mechanical model are obtained by our parameter study and originate also partially from the work for healthy human hearts in [1, 5]. All parameters are tabulated in Table 1. Finally, the fibre orientation map of the biventricular model, which is crucially attributing to the mechanics and electrical conduction system, is approximately calculated for the whole domain by linearly interpolating the local fibre angle on the endocardium ($+60^\circ$) to the local fibre angle on the epicardium (-60°) through the wall thickness [24].

Table 1: Material parameters for simulation of cardiac muscles of rat.

passive healthy	$a = 0.239$ kPa, $b = 9.683$, $a_f = 15.282$ kPa, $b_f = 15.277$, $a_s = 2.815$ kPa $b_s = 6.553$, $a_{fs} = 0.312$ kPa, $b_{fs} = 11.391$, $\kappa = 10^4$ kPa
passive infarcted	$a = 0.767$ kPa, $b = 9.506$, $a_f = 48.631$ kPa, $b_f = 14.669$, $a_s = 8.286$ kPa $b_s = 7.658$, $a_{fs} = 1.004$ kPa, $b_{fs} = 11.248$, $\kappa = 10^4$ kPa
active	$k_T = 0.49$ kPa mV^{-1} , $\Phi_r = -80$ mV, $\nu_{ff} = 1.0$, $\nu_{ss} = 0.1$
switch	$\epsilon_0 = 0.1$ mV^{-1} , $\epsilon_\infty = 1.0$ mV^{-1} , $\xi = 1.0$ mV^{-1} , $\tilde{\Phi} = 0$ mV
conduction	$D_{iso} = 0.1$ $\text{mm}^2 \text{ms}^{-1}$, $D_{ani} = 0.3$ $\text{mm}^2 \text{ms}^{-1}$
excitation	$\alpha = 0.01$, $\beta = 0.55$, $c = 8$, $\gamma = 0.002$, $\mu_1 = 0.2$, $\mu_2 = 0.3$, $G_s = 10$, $\phi_s = 0.6$
conversion	$\beta_\phi = 100$ mV, $\delta_\phi = 80$ mV, $\beta_t = 12.9$ ms

Simulation of myocardium To obtain the cardiac muscle contraction, the base plane is pinned on Γ_φ , see Figure 1. However, in reality, the base plane might be slightly displaced or twisted due to its interaction with surrounding tissues and its fibre direction contractions [2]. As seen in Figure 5, to trigger the myocardial excitation, several nodes (in red) on the endocardium close to the apex A (in green) are stimulated with a sufficiently high AP (-20 mV). Figure 5 shows the simulations of the healthy and infarcted models using the initial and boundary conditions given above, and the position of MI is

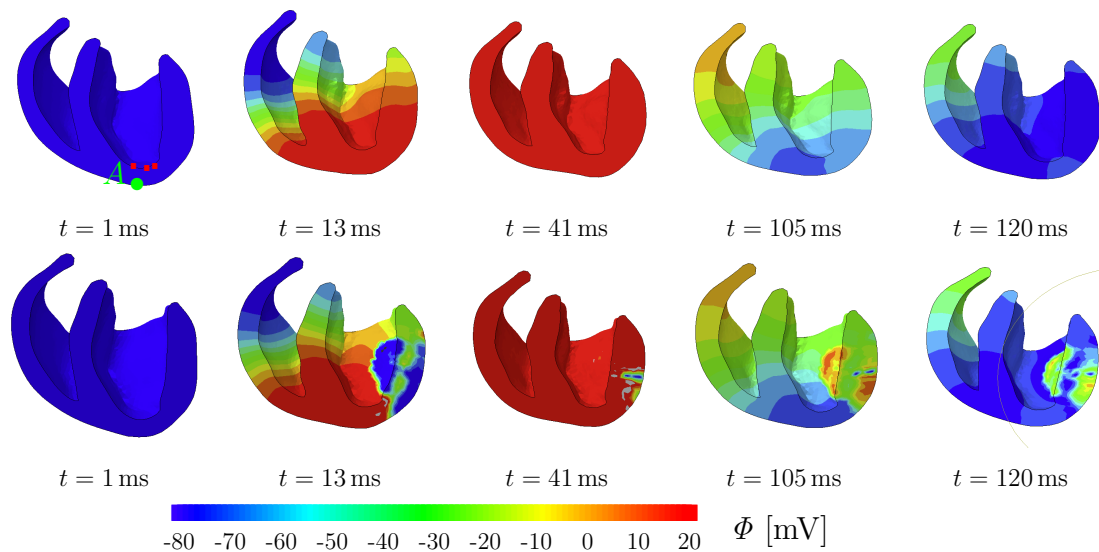


Figure 5: AP over time; depolarization and repolarization starting from apex A : healthy myocardium (1st row) and infarcted myocardium with delayed and complicated distribution of AP (2nd row).

illustrated in Figure 2. For both cases, the depolarization starts from the apex at $t = 2$ ms and runs to the base. At $t = 41$ ms, both models are excited at the peak of potential (+20mV) and start repolarization from the stimulated region near the apex at about $t = 105$ ms. However, for the healthy case, at $t = 13$ ms the whole myocardium becomes evenly excited while the infarcted region is still at the resting potential. The myocytes in the infarcted region cannot conduct the electrical wave. Thus, this region is excited with a delay and shows a decreased contraction. For the time points $t = 41, 105$ and 120 ms there are obviously significant differences in AP between the two cases. Consequently, a key effect of MI can also be seen in Figure 6, the infarcted region causes a smaller apex-to-base displacement. Obviously, the infarcted region affects the heart function and the heart muscles must contract faster and stronger to compensate the inactivated myocytes in the infarcted region in order to keep up with the same blood volume pumped through the body.

8 CONCLUSIONS

We present an electromechanical model for rat hearts and demonstrate an effective protocol to solve the partial/fully coupled problems to investigate healthy and diseased rat hearts. Our model can be used to study insights into physiology and pathology of the rat heart. Especially, the MEF is implemented and can be employed to investigate what affects physiology as well as

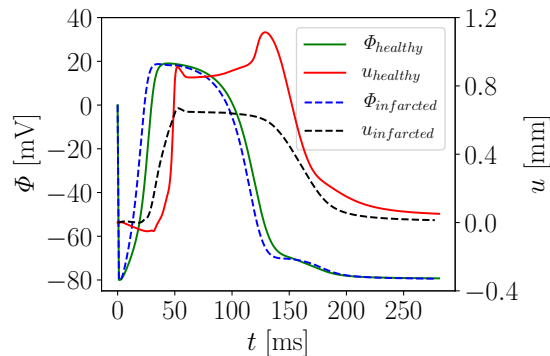


Figure 6: Evolution of AP Φ and displacement magnitude u of apical node A in healthy and infarcted models.

atrial and ventricular fibrillation. In the future, the model will be validated with ongoing experiments on rats to achieve more accurate response of the rat ventricular electromechanics. Furthermore, we plan to improve the model and take into account the heterogeneity of the myocardium as well as contribution of the Purkinje network in order to achieve more realistic behaviour of the heart.

Acknowledgements The authors thank the Klaus Tschira Stiftung grant 00.289.2016 for funding support.

REFERENCES

- [1] Baillargeon, B., Rebelo, N., Fox, D.D, Taylor, R.L. and Kuhl E. The living heart project: A robust and integrative simulator for human heart function. *European Journal of Mechanics, A/Solids*. (2014) **48**(1):38–47.
- [2] Asner, L. et al. Patient-specific modeling for left ventricular mechanics using data-driven boundary energies. *Computer Methods in Applied Mechanics and Engineering*. (2017) **314**(Supplement C):269–295.
- [3] Palit, A. et al. Computational modelling of left-ventricular diastolic mechanics: Effect of fibre orientation and right-ventricle topology. *Journal of Biomechanics*. (2015) **48**(4):604–612.
- [4] Carapella, V. et al. Quantitative study of the effect of tissue microstructure on contraction in a computational model of rat left ventricle. *PLOS One*. (2009) **9**(4):1–12.
- [5] Göktepe, S. and Kuhl, E. Electromechanics of the heart: a unified approach to the strongly coupled excitation-contraction problem. *Computational Mechanics*. (2010) **45**(2):227–243.
- [6] Holzapfel, G.A. and Ogden, R.W. Constitutive modelling of passive myocardium: a structurally based framework for material characterization. *Philosophical Transactions of the Royal Society of London A: Mathematical, Physical and Engineering Sciences*. (2009) **367**(1902):3445–3475.
- [7] Eriksson, T.S., Prassl, A.J., Plank, G. and Holzapfel, G. A. Modeling the dispersion in electromechanically coupled myocardium. *International Journal for Numerical Methods in Biomedical Engineering*. (2013) **29**(11):1267–1284.
- [8] Pluijmert, M. et al. Effects of activation pattern and active stress development on myocardial shear in a model with adaptive myofiber reorientation. *American Journal of Physiology-Heart and Circulatory Physiology*. (2014) **306**(4):H538–H546.
- [9] Hodgkin, A.L. and Huxley, A.F. A quantitative description of membrane current and its application to conduction and excitation in nerve. *The Journal of Physiology*. (1952) **117**(4):500–544.

- [10] Fitzhugh, R. Impulses and physiological states in theoretical models of nerve induction. *Biophys. J.* (1961) **1**:455–466.
- [11] Aliev, R.R. and Panfilov, A.V. A simple two-variable model of cardiac excitation. *Chaos, Solitons & Fractals.* (1996) **7**(3):293–301.
- [12] Kohl, P., Hunter, P. and Noble, D. Stretch-induced changes in heart rate and rhythm: clinical observations, experiments and mathematical models. *Progress in Biophysics and Molecular Biology.* (1999) **71**(1):91–138.
- [13] Frotscher, R. et al. Sample-specific adaption of an improved electro-mechanical model of in vitro cardiac tissue. *Journal of Biomechanics.* (2016) **49**(12):2428–2435.
- [14] Pandit, S.V. et al. A mathematical model of action potential heterogeneity in adult rat left ventricular myocytes. *Biophysical Journal.* (2001) **81**(6):3029–3051.
- [15] Teh, I. et al. Resolving fine cardiac structures in rats with high-resolution diffusion tensor imaging. *Scientific Reports.* (2016) **6**:30573.
- [16] Sirry, M.S., Ryan, J., Butler, B. and et al. Characterisation of the mechanical properties of infarcted myocardium in the rat under biaxial tension and uniaxial compression. *Journal of the Mechanical Behavior of Biomedical Materials.* (2016) **63**:252–264.
- [17] Niederer, S.A., Ter Keurs, H.E. and Smith, N.P. Modelling and measuring electromechanical coupling in the rat heart. *Experimental physiology.* (2009) **94**(5):529–540.
- [18] Treuting, P.M., Dintzis, S.M. and Montine, K. S. *Comparative Anatomy and Histology: A Mouse, Rat, and Human Atlas.* Elsevier, 2nd Edition, 2017.
- [19] Panfilov, A.V., Keldermann, R.H. and Nash, M.P. Self-organized pacemakers in a coupled reaction-diffusion-mechanics system. *Phys. Rev. Lett.* (2005) **95**(25):258104.
- [20] Mendis, S. et al. World Health Organization definition of myocardial infarction: 2008–09 revision. *International Journal of Epidemiology.* (2009) **40**(1):139–146.
- [21] Bogen, D.K. et al. An analysis of the mechanical disadvantage of myocardial infarction in the canine left ventricle. *Circulation Research.* (1980) **47**(5):728–741.
- [22] Nash, M.P. and Panfilov, A.V. Electromechanical model of excitable tissue to study reentrant cardiac arrhythmias. *Progress in biophysics and molecular biology.* (2004) **85**(2):501–522.
- [23] Dokos, S., Smaill, B.H., Young, A. and LeGrice, I.J. Shear properties of passive ventricular myocardium. *Heart and circulatory physiology.* (2002) **283**(6): H2650–H2659.
- [24] Wong, J. and Kuhl, E. Generating fibre orientation maps in human heart models using Poisson interpolation. *Computer Methods in Biomechanics and Biomedical Engineering.* (2014) **17**(11):1217–1226.